Heliyon 9 (2023) e17677

Contents lists available at ScienceDirect

Heliyon

journal homepage: www.cell.com/heliyon

Movement characteristics of the inclined surface flow of the open channel on the nanoscale surface

Yen-Chang Chen [a], Han-Chung Yang [b,*]

[a] Department of Civil Engineering, National Taipei University of Technology, Taipei, Taiwan, ROC
[b] Department of Marine Leisure Management, National Kaohsiung University of Science and Technology, Kaohsiung, Taiwan, ROC

ARTICLE INFO

Keywords:
Nanoscale
High-speed video system
Fiber-optic laser doppler velocimetry
Velocity profile
Open channel

ABSTRACT

This study investigates the water flow characteristics on a solid surface with nanoscale compared to a normal solid surface. The experiment uses a high-speed video system and Fiber-optic Laser Doppler Velocimetry to measure the flow condition of the droplet and velocity distribution profile in the inclined surface flow of the open channel, respectively. The results showed that the movement speed of water droplets on the nanoscale surface was about 2 times faster than on the normal surface. The mean error of each velocity profile was 0.6%. The results reveal that the velocity profile is not significantly influenced by whether the flume bottom is coated with nanoscale material or not in the inclined surface flow of the open channel.

1. Introduction

Understanding the movement characteristics of water flow in an open channel is essential to comprehend the changes in water velocity, flow discharge, and water level. This can provide scientific evidence for fields such as hydraulic engineering and water resource management, which are crucial for designing and managing hydraulic projects [1]. Investigating the changes in flow patterns, velocity distribution, and turbulence characteristics of water flow can lay the foundation for related hydrological and hydraulic research. Additionally, water flow in open channels often varies due to different material surfaces [2]. In terms of flow velocity, the flow velocity is lower on rough surfaces due to higher friction resistance and more apparent energy dissipation. Conversely, the flow velocity is higher on smooth surfaces due to lower friction resistance. The suspended particles in water also accumulate differently depending on the flow velocity. Smooth surfaces are less likely to result in particle deposition. However, when the material surface exhibits a lotus effect, studying and exploring how this will affect the movement characteristics of water flow in an open channel is necessary.

Barthlott and Neinhuis [3] discovered the relationship between hydrophobicity and the self-cleaning mechanism of many biological surfaces, which led to the discovery of the theory of the "Lotus Effect." The Lotus-Effect theory [4–6], derived from the superhydrophobic surface and self-cleaning characteristics of lotus leaves, explains that when water lands on a fluid-repellent surface, it tensions to become spherical droplets. In physics, when a contact angle of water and a fluid-repellent surface is more significant than 140°, even at the slightest tilt, the water turns to drops and independently rolls off. Observing a lotus leaf under an electronic microscope, a micro relief of epidermal cells about 5–15 μm in height can be seen coated with a layer of wax crystal about 1 nm in diameter [7]. The chemical composition of this wax crystal causes effective water repellency, minimizes the contact area, and

* Corresponding author.
E-mail addresses: yenchen@ntut.edu.tw (Y.-C. Chen), hanchung@nkust.edu.tw (H.-C. Yang).

https://doi.org/10.1016/j.heliyon.2023.e17677
Received 1 February 2023; Received in revised form 27 April 2023; Accepted 25 June 2023
Available online 26 June 2023

maximizes the contact angle when water lands on such surfaces. Hence even after torrential rain, the surfaces of lotus leaves always remain waterless; at the same time remain spotless by the self-cleaning process of running off quickly, picking up contaminating residues, and eventually rolling off, which is precisely the reason why lotus is the symbol of purity [8].

The terms for a nanoscale solid boundary in designing and manufacturing are known as hydrophilic and hydrophobic or lipophilic and oleophobicity, so-called "Binary Cooperative Complementary Nanoscale Interfacial Materials" commonly seen materialized in many everyday products [9]. This "Binary Cooperative Complementary Nanoscale Interfacial Materials" implies a unique coating process on material surfaces, enabling materials to perform uniquely. This nanotechnology is utilized to produce substances that have both superhydrophilic and superhydrophobic qualities simultaneously. For instance, the surfaces of glass and building materials processed in such technology have self-cleaning and defogging functions [9–11].

Nanotechnology has been researched constantly to be used innovatively, such as by Fernandes et al. [12], Subramanian & Lee [13], Lee et al. [14], Bumataria et al. [15], and Gbadeyan et al. [16]. Meanwhile, whether the effect of open channel flow contacting a nanoscale solid boundary concludes in the same result as a regular surface is worth investigating and being enlightened. Due to the viscosity between fluid and solid boundaries, when fluid at a solid wall commonly forms into one of the "no-slip" conditions [17,18], that is, the velocity of a fluid on the solid surface is zero. Nevertheless, other studies and research done in the past prove that the "no-slip" condition is not necessarily actual in all situations of fluid flowing on surfaces of hydrophilic and hydrophobic solid boundaries. Tretheway and Meinhart [19] exploit a micron-resolution particle image velocimetry device to measure the velocity profiles of fluid flowing in 30 × 300 μm microchannels and point out the dissimilarities on the surfaces of hydrophobic and hydrophilic boundaries. For instance, compared with a hydrophilic surface, a difference of about 10% of the velocity is measured when the microchannel surface is smeared with a 2.3 nm thick layer of hydrophobic material. In addition, the velocity of a fluid on a solid surface of a hydrophobic materialized microchannel does not measure to be zero, and a slip occurs at the wall of approximately 1 μm in length. This is to say that the "no-slip" condition is not necessarily accepted in a hydrophobic material's microchannels but is determined by the characteristics of the fluid and solid boundary surfaces. Craig et al. [20], Schäffel et al. [21], and more scientists have published research regarding the measuring technique of slip velocity under different conditions of fluid flowing on hydrophilic or hydrophobic surfaces and find slip lengths are less than 1 μm in average.

Most studies, including many mentioned above, are done on a micro-scale to obtain the characteristics of microchannels. However, what happens when a macro-scale water body under a much more significant influence of gravity, such as open channel flows, flowing on solid boundaries materializes differently? Most of the previous related studies did not mention this issue and results, such as Ramesh et al. [22], Greco & Moramarco [23], Daneshfaraz et al. [24], Parsamehr et al. [25]. To uncover the doubt, we must do relevant experimental design and measurement studies on this research subject to comprehend the issues that may arise due to actual applications and then master the impact and scope of nanotechnology developments. This is the critical objective of this study.

In this study, a high-speed video system and the Fiber-optic Laser Doppler Velocimetry (FLDV) are used to measure the flow condition of the droplet and the velocity distribution profile in the inclined surface flow of the open channel, respectively. This study intends to understand whether there is a correlation between the characteristics of solid boundary material and fluid adhesion by observing the specifics of water drop and inclined surface flow movements on a nanoscale surface, then comparing it with a general hydrophilic materialized surface. Therefore, the contribution of this study will provide an essential basis for the selection of different surface materials in the design and management of open channel engineering to ensure the safety and sustainable development of hydraulic engineering. This research will also provide innovative ideas related to large-scale (open channel) water flow.

2. Materials and methods

2.1. Hydrophobic coating material - Teflon® AF

Due to Teflon® AF's fluoropolymer provides fine qualities of low dielectric constant, weak factor, etc., and is the lowest electric

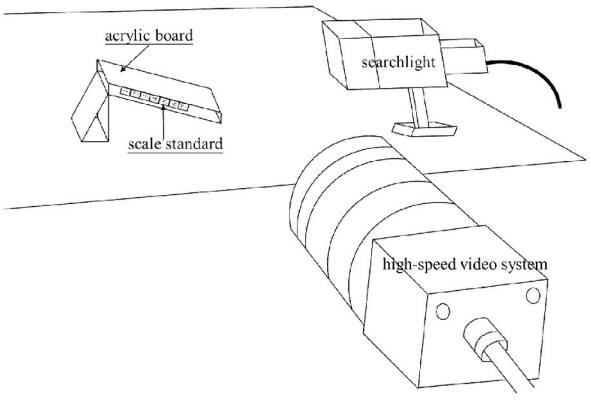

Fig. 1. The experimental equipment for water drop movement.

conductor among all malleable plastics [26]. Teflon® AF's extreme stability enables it to reduce contractions of molds, and under high temperatures, it does not easily become fluidity or heat conducting because of its durability and heat resistance. Since Teflon® AF does not dissolve in any fluid [27], it can be ideal as a hydrophobic coating material. Thus to observe, measure, and analyze the movements and velocities of water drop and inclined surface flow on a nanoscale surface, Teflon® AF is selected to design a hydrophobic solid surface for the experiment.

2.2. Experimental method for water drop movement

Besides the hydrophobic material, Teflon® AF, a ventilator, steel trays, steel clips, gloves, acrylic boards, suction bulbs, and so forth were utilized in experimenting with water drop movements on the hydrophobic surface. As coating Teflon® AF for the experiment must be done in a ventilated environment, a negative pressure ventilating system was used mainly to pump air out within the ventilator through a highly efficient filter screen. The ventilator sifted air outdoors at a minimum speed of 75 ft/min. A safety suction bulb was to deliver a moderate amount of Teflon® AF to the steel tray, then to avoid direct contact with the acrylic board coated in Teflon® AF; besides wearing gloves, steel clips were utilized as taking tools. Then only one side of the acrylic board was immersed in the tray filled with the needed amount of Teflon® AF. The acrylic board acted as an important solid boundary between the fluid and Teflon® AF, and Teflon® AF as an interface between fluid (water drops) and solid (acrylic board). Fig. 1 illustrates more experimental equipment used in this study, such as a high-speed video system, searchlight, acrylic board, and scale standard. The light source chosen for this study is a halogen lamp, and the position of the light will vary due to the conditions of the research site at that time, and it needs to be adjusted to a place where the image can be captured clearly. After adjusting the focal light source and confirming that the captured water droplets are clear, the high-speed video system is turned on to capture the required images quickly.

2.3. Experimental method for inclined surface flow

The equipment used to circulate the water to create an open channel flow effect, including a standard pressure water tank, a flume, and a water tank. The standard pressure water tank was facilitated with an overflow function to stabilize the pressure head. The top of the tower is covered with a stainless steel cover to prevent foreign objects and dust in the air from entering. The flume was 12 m in length, 0.5 m in width, and 0.5 m in depth. Two sides and the bottom platform were made in 1 cm thick translucent glass to avail the Fiber-optic Laser Doppler Velocimetry measurement proceedings. It was adjustable to incline within 0%–10%, and an adjustable flowmeter controlled discharges. A falling water method was employed to accumulate the tailwater into the last water tank of the circulation; then a water pump was to send water to the rooftop water tank; finally, let gravity took its course and flowed to the standard pressure water tank to finish the complete cycle. The velocity measuring device was a two-color, two-component, four-beam Fiber-optic Laser Doppler Velocimetry made by an American company. The measuring system was sorted into six divisions: a set of

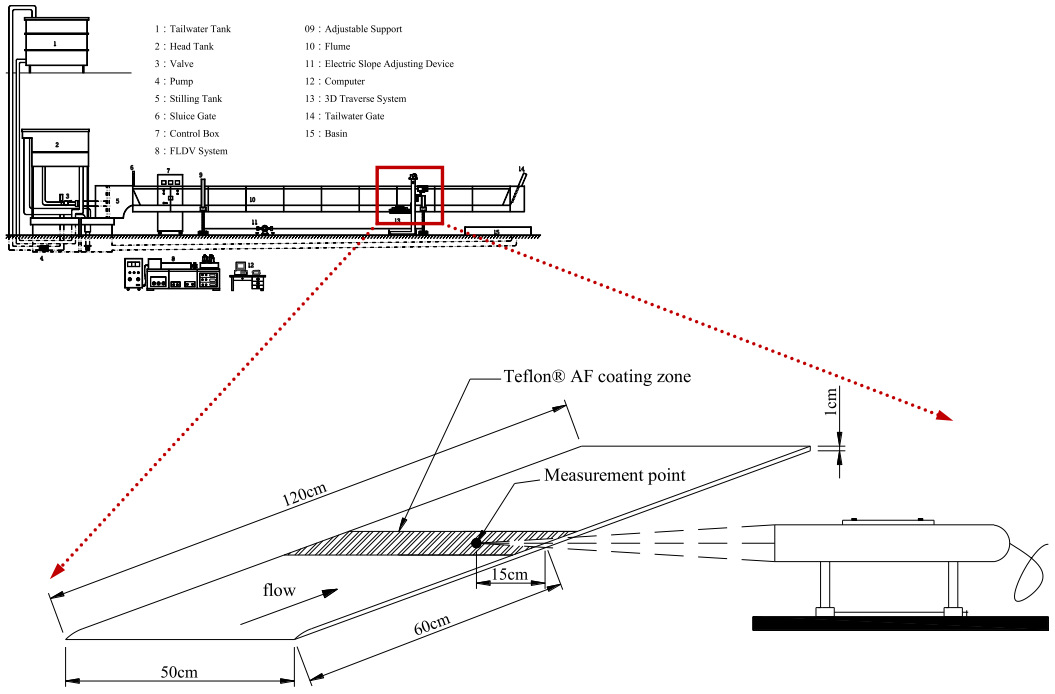

Fig. 2. The experiment equipment for open channel flow.

laser photo sources, a color burst or multicolor beam separator, a fiber-optic probe, a color link or multicolor receiver, a group of signal processors, and a systematic control computer software. The detector was operated and moved by a three-dimensional traverser, which precision can reach 0.001 mm, and its focusing lens could converge four beams of light into a point. A Doppler alert was projected to the detector's fiber-optic receptor and the color link when an aerosol pellet passed through this crossing point. The received signal was magnified and sent to the signal processor to filter any noise for analysis [28].

The mean velocity profiles of open channel flow in flume bottoms coated with and without Teflon® AF were compared and contrasted. A flat acrylic board of 120 cm in length by 50 cm in width was placed on the bottom of the flume. There is a gradient segment in front of the board. The mean velocity profile measuring position was located at 60 cm from the front edge of the board and against the right bank wall of 15 cm. The Teflon® AF was coated 50–70 cm away from the front edge and the right to the left bank within the proximity. The fiber laser Doppler Velocimetry system measured the mean velocity profile, and the detailed configuration is shown in Fig. 2. The flow conditions of the two groups of experiments (RUN 1 and RUN 2) were controlled at 2 cm in water depth (H), 28 °C in water temperature (T), and 0.5% in channel slope (S). RUN1 indicates without Teflon® AF coating and RUN2 with the coating. In RUN 1, U_m (the mean velocity) is 0.429 m/s, U_* (the friction velocity) is 0.03 m/s, Reynold's number (U_mR/ν; where R refers to Hydraulic radius; ν refers to kinematic viscosity) is 9464, and Froude's number ($U_m/\sqrt{gH}$; where g is Acceleration of gravity) is 0.969. In RUN 2, U_m is 0.431 m/s, U_* is 0.03 m/s, Reynold's number is 9508, and Froude's number is 0.973. The conditions of each run of experiments are shown in Table 1.

3. Results and analyses for water drop

In this part of the study, the water drop movements on the acrylic boards coated in Teflon® AF and without are compared. The research mainly discusses the difference in the contact angle of water droplets when the level is stationary and the movement of water droplets when there is a slope.

3.1. Water drop contact angles

The magnitude of the contact angle was generally utilized to determine whether a solid surface material was hydrophilic or hydrophobic [29]. If a static state contact angle of water drop on a material surface was greater than 90°, the material was hydrophobic and called a hydrophobic surface. Whereas a contact angle was less than 90°, the material was hydrophilic and called a hydrophilic surface [30].

After producing a hydrophobic solid surface with hydrophobic material Teflon® AF, water was dropped respectively on the surface with and without Teflon® AF and then recorded with a high-speed video system to measure each contact angle respectively. In the case of the acrylic board without Teflon® AF coating, the contact angle was 70°, as shown in Fig. 3. While the contact angle was 105° when the water drop landed on the board surface coated with Teflon® AF, as shown in Fig. 4. This result matched precisely with the information provided by DuPont company. This result also showed that a hydrophobic solid surface production technology is feasible in this study.

3.2. Characteristics of water drop movement

To fully comprehend the characteristics of water drop movement, in this study, plastic shavings were sprinkled respectively on the surfaces with and without Teflon® AF coating, and the boards were tilted at a 20° angle purposely to examine not only the movements on slopes but also the effects of a self-cleaning mechanism.

Fig. 5 displays water drops on the surface of the acrylic board without Teflon® AF coating. The water drop slipped rather than rolled noticeably in slow motion during this experiment. Also, when the water drop encountered the plastic shavings, it could only pick up a minimal amount and left some water behind due to adhesion. Fig. 6 shows, in contrast, water drops on the surface of the hydrophobic boundary. The unique quality of the movement in this situation was how it rolled. Unlike Fig. 5, the water drop successfully picked up plastic shavings on the surface as it rolled off. Figs. 7 and 8 separately exhibit the continuous movements of water drops on the surface with and without Teflon® AF coating in a series of photos by high-speed camerawork. The fragment of time filmed for Fig. 7 was 2.6 s and 1.3 s for Fig. 8. In comparing Figs. 7 and 8, it was evident that the water drop moved much faster on the surface with Teflon® AF coating than without under the same given circumstances.

Due to a greater cohesion of the water molecule, there was a relatively smaller adhesion between the water molecule and the acrylic

Table 1
Experiment condition for open channel flow.

Run	U_m (m/s)	U_* (m/s)	Re	Fr
RUN1 (without Teflon)	0.429	0.03	9464	0.969
RUN2 (with Teflon)	0.431	0.03	9508	0.973

Note: U_m = Mean velocity, U_* = Friction velocity, Re = Reynold's number (= U_mR/ν), Fr = Froude number (= $U_m/\sqrt{gH}$), R = Hydraulic radius, ν = Kinematic viscosity, g = Acceleration of gravity.

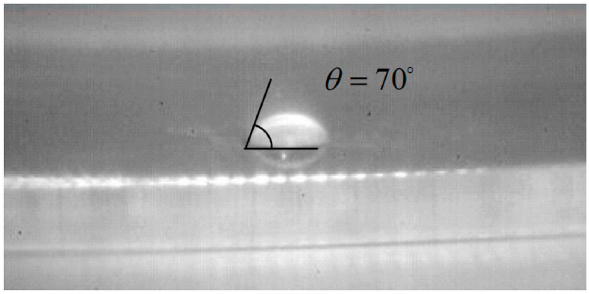

Fig. 3. The acrylic board without Teflon® AF coating, the contact angle is 70°.

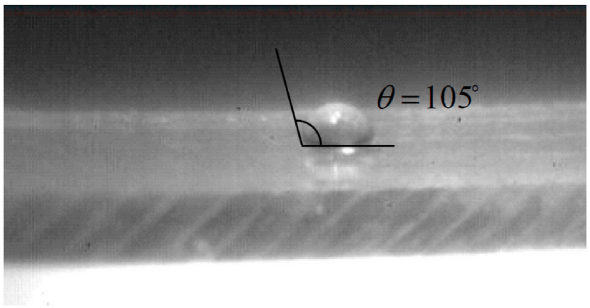

Fig. 4. The acrylic board with Teflon® AF coating, the contact angle is 105°.

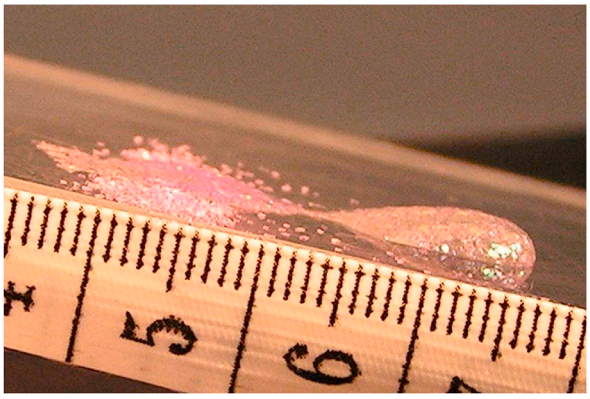

Fig. 5. Water drops on the surface of the acrylic board without Teflon® AF coating.

board; and the water rolled down because the board inclination angle was greater than a still angle. The known dynamic viscosity $\mu = \frac{F}{A_i} \cdot \frac{\partial L}{\partial V}$: F represents the force; L is the length; A_i is the interfacial area, and V is the velocity of the water drop [31]. According to the formula, when μ, F, *and* L values are fixed, there is an inverse ratio between the velocity and the interfacial area. In other words, it runs down faster when water turns to a spherical droplet (or a hydrophobic stage) because its interfacial area becomes smaller. On the contrary, when water forms into a half-spherical droplet (or a hydrophilic stage), the interfacial area becomes larger and slides downward at a slower speed. In addition, when water drops on a hydrophobic surface, it turns into a spherical droplet due to a greater contact angle and a smaller interfacial area, then starts to slope downward with the help of gravity in the movements of a sphere. Also, because of the adsorption, the water drop quickly picks up plastic shavings and cleans as it rolls away. From this experiment, we perceived different results from water drops on the hydrophobic coating material of Teflon® AF and the regular surface. Also, we believe that this is the reason for the self-cleaning effect of hydrophobic surfaces.

3.3. Discussion

This study utilizes Teflon® AF to produce a hydrophobic surface. The experiment demonstrates that water drops on hydrophobic surfaces tend to form a spherical droplet due to the greater contact angle and smaller interfacial area. This spherical shape and the lack

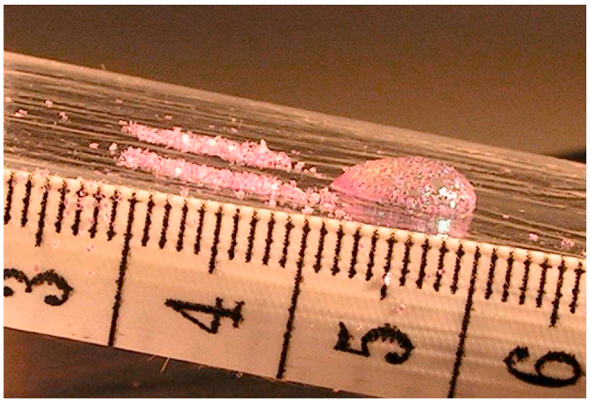

Fig. 6. Water drops on the surface of the acrylic board with Teflon® AF coating.

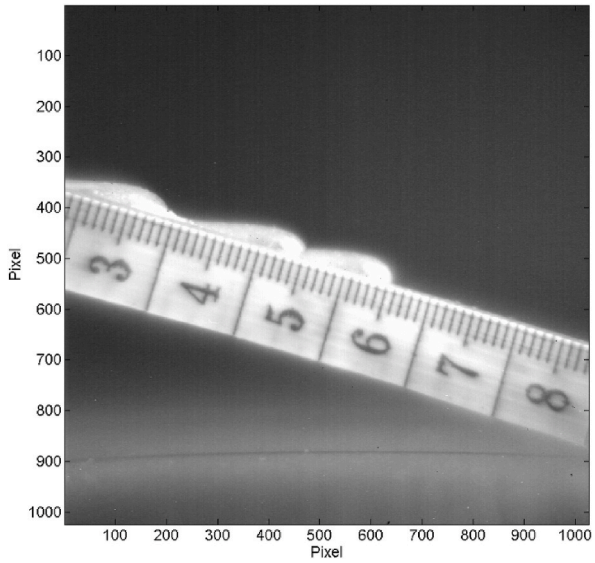

Fig. 7. The continuous movements of water drop on the surface without Teflon® AF.

of adhesion allow the water drop to roll off the surface faster, carrying away any dirt or debris and resulting in a self-cleaning effect. The results of this study provide insights into the behavior of water drops on hydrophobic and hydrophilic surfaces and how it relates to the self-cleaning mechanism. It also verified the results of previous related studies-for example, Heckenthaler et al. [32]. The self-cleaning properties of hydrophobic surfaces could be utilized to reduce maintenance costs and improve the efficiency of various systems. For example, hydrophobic coatings on building materials can prevent the accumulation of dirt and dust, enhancing the material's lifespan and reducing cleaning expenses [33].

4. Results and analyses for inclined surface flow

The characteristics of water drop movement on a hydrophilic and hydrophobic surface are distinct, learning from the above experimentation. However, when all the water droplets gather to form a water flow, whether there is any difference in the flow velocity distribution of the water flowing on the surface of the hydrophilic and hydrophobic channels, the experimental results will be explained below.

4.1. Mean velocity distribution

The velocity profile of water flow is one of the essential items to study the movement mechanism of the overall open channel flow, which can present the water flow's microscopic and macroscopic movement characteristics. Its velocity profile is generally divided into inner and outer regions for an open channel flow with a free water surface. Considering that the movement characteristics of water flow differ, the inner region can be divided into viscous sublayer and wall region. In the inner region, the mean velocity profile is

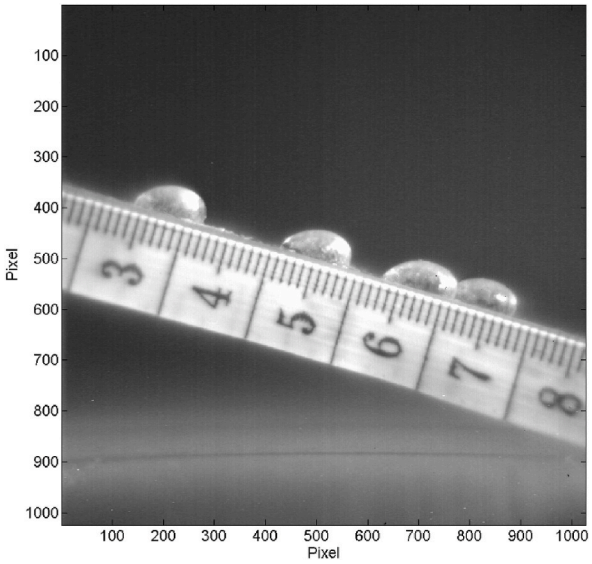

Fig. 8. The continuous movements of water drop on the surface with Teflon® AF.

mainly controlled by parameters such as bed shear stress, fluid viscosity, and height from the bed. Thus the mean velocity distribution in the viscous sublayer is shown below [34].

$$U^+ = Y^+ \ (Y^+ < 5) \tag{1}$$

In formula (1), $U^+ = \frac{u}{U_*}$ is the dimensionless mean velocity in the mainstream direction, $Y^+ = \frac{U_* y}{\nu}$ is the friction Reynold's number, y is the height from the bed, u is the flow velocity in the mainstream direction, $U_* = \sqrt{\tau_0/\rho}$ is the friction velocity, ν is the kinetic viscosity, τ_0 is the bed shear stress, ρ is the fluid density.

In the wall region, one of the most popular velocity distribution models is the log-law presented by Prandtl [35], and Einstein [36], as shown below.

$$U^+ = \frac{1}{\kappa} \ln Y^+ + A \ (Y^+ > 30) \tag{2}$$

In formula (2), κ is a von Karman constant, and A is an integral constant. Many scholars have conducted theoretical analysis and experimental research to obtain different κ and A values for the smooth open channel flow conditions, as shown in Table 2.

Under the identical measuring position and flowing condition, the velocity profiles, respectively, with and without Teflon® AF coating, are demonstrated in Fig. 9. The hollow dot designates the measured result of the velocity distribution profile without Teflon® AF coating, and the hollow square is with the coating in the figure. Judging from the figure, the overall results appear almost identical, and the few variations are within the permissible deviation range. The mean error of each velocity profile was at 0.6% (by $\sum_{i=1}^{n}((NoTef - Tef)/NoTef)/n$, which *NoTef* and *Tef* correspondingly specifies the hydrodynamics of water flowing on the flume bottoms without and with hydrophobic material, n as an integer). Additionally, every experimental data was compared with the Law of the Wall, as seen in Fig. 10, U^+ is to u/U_*, and Y^+ is to $U_* y/\nu$. The figure explains that if the viscosity layer is within $Y^+ < 5$, the velocity profile is not significantly influenced by whether or not the flume bottom is coated with a hydrophobic material. While on the near wall area ($Y^+ > 30\,; y/H < 0.2$), the velocity distribution profile matched the log-law. Thus the regression analysis was used to estimate and obtain $\kappa = 0.487$ (von Karman constant in log-law), $A = 6.21$ (an integral constant), and R-squared $= 0.999$.

Based on Shannon's [43] entropy theory, Chiu [44,45] integrated it into the flow velocity distribution of open channel flow from the probability perspective and derived Chiu's flow velocity distribution, as shown below.

Table 2
Overview of previous studies on κ and A values in smooth open channel flow.

Scholar	κ	A
Keulegan [37]	0.400	5.50
Steffler et al. [38]	0.400	5.50
Nezu & Rodi [39]	0.412	5.29
Kirkgöz [40]	0.410	5.50
Cardoso et al. [41]	0.401	5.10
Dong et al. [42]	0.400	6.00

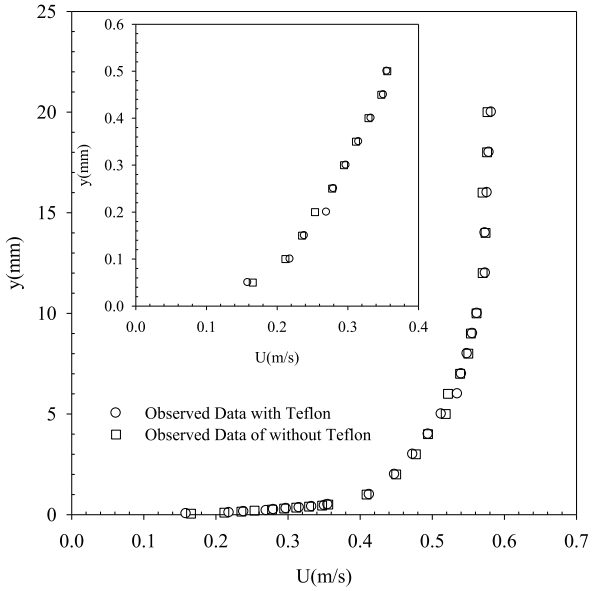

Fig. 9. The Observed velocity of Teflon® AF Bottom and without Teflon® AF Bottom.

$$u = \frac{U_{\max}}{M} \ln\left[1 + \left(e^{M} - 1\right)\frac{\xi - \xi_0}{\xi_{\max} - \xi_0}\right] \tag{3}$$

In formula (3), M is the entropy parameter and ξ is the dimensionless coordinate of the flow velocity distribution. $\xi_{\max}$ and ξ_0 is the ξ value at $u = u_{\max}$ and $u = 0$, respectively. The physical meaning of $(\xi - \xi_0)/(\xi_{\max} - \xi)$ is the ratio of the area where the velocity is lower than u to the total area in the velocity distribution. In this study, the measured flow velocity distribution values are brought into this formula to analyze the flow velocity distribution. From Fig. 11, it can be seen that Chiu's flow velocity distribution can well represent all the measurement data in the viscous sublayer and wall region. This result shows that Chiu's flow velocity distribution formula can better represent the measured flow velocity distribution than that shown in Fig. 10.

4.2. Intensity of turbulence

An intensity of turbulence reflects the characteristics of a flow field, meaning it is a valuable parameter in analyzing a flow field. Hence, a further explanation of the turbulence intensity profile of open channel flow flowing on flume bottoms coated with and without Teflon® AF is described here. Nezu & Rodi [39] used a laser Doppler anemometer to study the smooth open channel flow field and proposed an empirical model to describe turbulence intensity distribution in the main direction. When $Y^+ > 30$, the turbulence intensity distribution in the main direction can be expressed by the following formula.

$$\frac{u'}{U_*} = D_u \cdot \exp\left(-\lambda_u \cdot \frac{y}{H}\right) \tag{4}$$

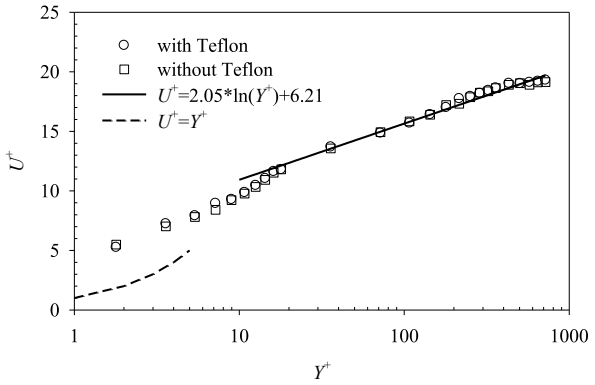

Fig. 10. Experiment data compared with log-law.

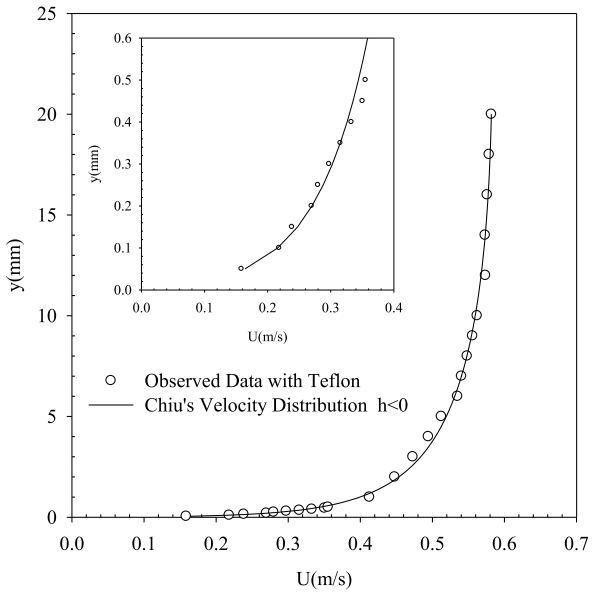

(a) Run1

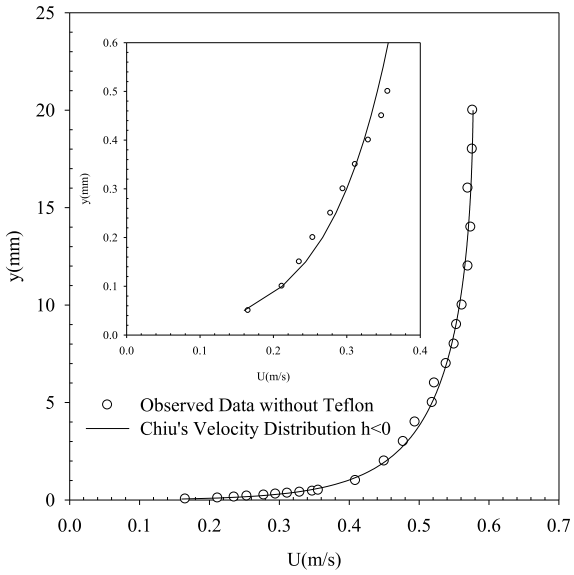

(b) Run2

Fig. 11. The Chiu's velocity distribution of (a) Run1 (b) Run2.

In the formula, u' is the turbulence intensity in the main direction, and D_u and λ_u are empirical constants. Nezu & Nakagawa [46] used a hot-film anemometry to obtain the experimental data of formula (4) to study open channel flows. After analysis, the values of empirical constants D_u and λ_u were 2.3 and 1.0, respectively. Fig. 12 illustrates the relationship between the mainstream turbulence intensity (u'/U_*) and Y^+. As seen in the figure, when water flow conditions remain the same, but flume bottoms are not the same, the experiment results in the near wall and outer area ($Y^+ > 30$) were almost consistent. The mean error percentage was 1.8%, which means that the mainstream to turbulence intensity was not affected by different conditions of the flume bottom. In the case of $Y^+ < 5$ the viscosity layer, the results also showed no apparent changes; the mean error percentage also stayed at 1.8%. Fig. 13 changes Y^+ to the relative height y/H and compares it with the formula of Nezu and Nakagawa [46]. Within the range $y/H > 0.1$, the mean error percentage between the trial and the formula was 14%; however, it became 1% when the coefficient in the formula was changed to 2.0.

4.3. Discussion

The results presented in this section demonstrate that a hydrophobic coating on the bottom of the flume does not significantly affect the velocity distribution profile in the viscous sublayer and wall region. This suggests that the hydrophobic coating does not affect the boundary layer behavior in this region. The Law of the Wall and Chiu's flow velocity distribution formula also provide a good fit for the experimental data in these regions. These findings have important implications for the design and operation of hydraulic structures and can be used to understand the behavior of fluids in the presence of hydrophobic coatings. The research content presented in this passage provides valuable insights into the turbulence intensity profile of inclined surface flow on flume bottoms with and without Teflon® AF coating. One finding from this research is that the mainstream turbulence intensity is not significantly affected by different conditions of the flume bottom. However, the results of this study are not necessarily applicable to experiments or research situations of small-scale (microchannel) water flow fields.

5. Conclusion

Through image analyses, we found that a water drop on an inclined hydrophobic surface moved in a rolling motion and at a higher velocity, which differentiated from a hydrophilic surface. However, when using the FLDV system to observe inclined surface flow on hydrophilic and hydrophobic surfaces, we noticed that the hydrodynamics of velocity distribution and turbulence intensity were not much influenced by hydrophobic coating material, and learned that each resulted in an almost identical manner. Especially under the nearest solid surface ($Y^+ < 5$), the dissimilarities of contact angle and flowing velocity seen in water drops on hydrophilic and hydrophobic materials were nearly non-existing, most likely caused by weight, pressure, and other characteristics of channel flow. In the macro-scale experimental results, this study suggests that there is no need to consider the effect of nanoscale (hydrophilic or hydrophobic) materials on water flow movement characteristics when constructing open channel flow facilities. Further research could explore the impact of hydrophobic coatings on the velocity distribution profile in other flow regimes or under different conditions, such as with various fluids. Additionally, more investigations could be conducted to explore the practical applications of hydrophobic coatings in hydraulic structures, such as reducing frictional losses to achieve the effect of energy saving.

Author contribution statement

Yen-Chang Chen: Conceived and designed the experiments; Contributed reagents, materials, analysis tools or data; Wrote the paper.

Han-Chung Yang: Conceived and designed the experiments; Performed the experiments; Analyzed and interpreted the data; Contributed reagents, materials, analysis tools or data; Wrote the paper.

Funding Statement

The APC was funded by National Kaohsiung University of Science and Technology.

Data availability statement

Data will be made available on request.

Declaration of competing interest

The authors declare that they have no known competing financial interests or personal relationships that could have appeared to

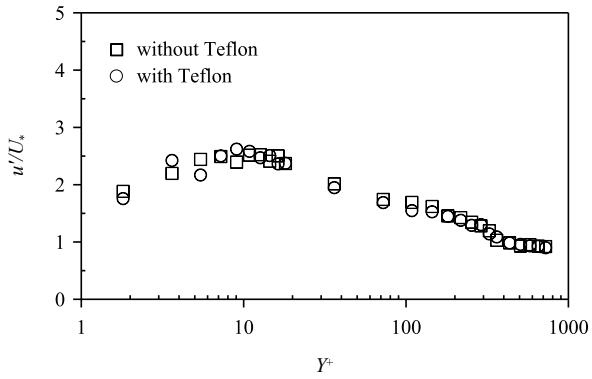

Fig. 12. Relationship between the mainstream to turbulence intensity.

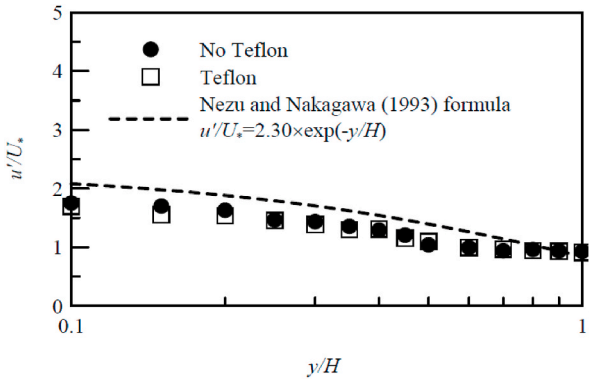

Fig. 13. Relationship between the mainstream to turbulence intensity.

influence the work reported in this paper

Acknowledgment

The authors would like to thank the National Science and Technology Council, Taiwan, for their financial support of this research under Contract NSC 93-2211-E-027-007 and thanks to Professor J. Y. Lu from Dept. of Civil Engineering, National Chung-Hsing Univ.

Notations

H	Water depth (L)
T	Water temperature
S	Channel slope
U_m	Mean velocity (LT^{-1})
U_*	Friction velocity (LT^{-1})
Re	Reynold's number
Fr	Froude number
R	Hydraulic radius (L)
ν	Kinematic viscosity (L^2T^{-1})
g	Acceleration of gravity (LT^{-2})
μ	Dynamic viscosity ($ML^{-1}T^{-1}$)
F	Force (MLT^{-2})
L	Length (L)
Ai	Interfacial area (L^2)
V	Velocity of the water drop (LT^{-1})
U^+	Dimensionless mean velocity in the mainstream direction
Y^+	Friction Reynold's number
y	Height from the bed (L)
u	Flow velocity in the mainstream direction (LT^{-1})
τ_0	Bed shear stress ($ML^{-1}T^{-2}$)
ρ	Fluid density (ML^{-3})
κ	von Karman constant
A	Integral constant
n	Integer
M	Entropy parameter
ξ	Dimensionless coordinate of the flow velocity distribution
ξ_{max}	ξ value at $u = u_{max}$
ξ_0	ξ value at $u = 0$
u'	Turbulence intensity in the main direction (LT^{-1})
D_u	Empirical constant
λ_u	Empirical constant

References

[1] P.K. Singh, P. Dey, S.K. Jain, P.P. Mujumdar, Hydrology and water resources management in ancient India, Hydrol. Earth Syst. Sci. 24 (10) (2020) 4691–4707.
[2] D.W. Knight, C. Hazlewood, R. Lamb, P.G. Samuels, K. Shiono, Practical Channel Hydraulics: Roughness, Conveyance and Afflux, CRC Press, 2018.
[3] W. Barthlott, C. Neinhuis, Purity of the sacred lotus, or escape from contamination in biological surfaces, Planta 202 (1) (1997) 1–8.
[4] M. Nosonovsky, P.K. Rohatgi, Lotus effect and self-cleaning, in: Biomimetics in Materials Science, Springer, New York, NY, 2011, pp. 319–341.
[5] C.J. Zhou, D. Tian, J.H. He, What factors affect lotus effect? Therm. Sci. 22 (4) (2018) 1737–1743.
[6] J. Li, W. Jiao, Y. Wang, Y. Yin, X. He, Spraying pressure-tuning for the fabrication of the tunable adhesion superhydrophobic coatings between Lotus effect and Petal effect and their anti-icing performance, Chem. Eng. J. 434 (2022), 134710.
[7] G. Acikbas, N. Calis Acikbas, The effect of sintering regime on superhydrophobicity of silicon nitride modified ceramic surfaces, J. Asian Ceram. Societies 9 (2) (2021) 734–744.
[8] F. Geyer, M. D'Acunzi, A. Sharifi-Aghili, A. Saal, N. Gao, A. Kaltbeitzel, et al., When and how self-cleaning of superhydrophobic surfaces works, Sci. Adv. 6 (3) (2020), eaaw9727.
[9] M. Liu, L. Jiang, Dialectics of nature in materials science: binary cooperative complementary materials, Sci. China Mater. 59 (4) (2016) 239–246.
[10] L. Jiang, R. Wang, B. Yang, T.J. Li, D.A. Tryk, A. Fujishima, K. Hashimoto, D.B. Zhu, Binary cooperative complementary nanoscale interfacial materials, Pure Appl. Chem. 72 (1–2) (2000) 73–81.
[11] R. Fang, M. Liu, L. Jiang, Progress of binary cooperative complementary interfacial nanomaterials, Nano Today 24 (2019) 48–80.
[12] T. Fernandes, L. Duester, F. Gottschalk, B. Gaiser, Contributors to the environmental nanotechnology themed issue, J. Environ. Monit. 13 (2011) 1132–1134.
[13] V. Subramanian, T. Lee, Nanotechnology-based flexible electronics, Nanotechnology 23 (34) (2012), 340201.
[14] C.H. Lee, B. Tiwari, D. Zhang, Y.K. Yap, Water purification: oil–water separation by nanotechnology and environmental concerns, Environ. Sci.: Nano 4 (3) (2017) 514–525.
[15] R.K. Bumataria, N.K. Chavda, H. Panchal, Current research aspects in mono and hybrid nanofluid based heat pipe technologies, Heliyon 5 (5) (2019), e01627.
[16] J.A. Gbadeyan, E.O. Titiloye, A.T. Adeosun, Effect of variable thermal conductivity and viscosity on Casson nanofluid flow with convective heating and velocity slip, Heliyon 6 (1) (2020), e03076.
[17] A.P. Bowles, C.D. Honig, W.A. Ducker, No-slip boundary condition for weak Solid− liquid interactions, J. Phys. Chem. C 115 (17) (2011) 8613–8621.
[18] I. Marusic, S. Broomhall, Leonardo da Vinci and fluid mechanics, Annu. Rev. Fluid Mech. 53 (2021) 1–25.
[19] D.C. Tretheway, C.D. Meinhart, Apparent fluid slip at hydrophobic microchannel walls, Phys. Fluid. 14 (3) (2002) L9–L12.
[20] V.S. Craig, C. Neto, D.R. Williams, Shear-dependent boundary slip in an aqueous Newtonian liquid, Phys. Rev. Lett. 87 (5) (2001), 054504.
[21] D. Schäffel, K. Koynov, D. Vollmer, H.J. Butt, C. Schönecker, Local flow field and slip length of superhydrophobic surfaces, Phys. Rev. Lett. 116 (13) (2016), 134501.
[22] R. Ramesh, B. Datta, S.M. Bhallamudi, A. Narayana, Optimal estimation of roughness in open-channel flows, J. Hydraul. Eng. 126 (4) (2000) 299–303.
[23] M. Greco, T. Moramarco, Influence of bed roughness and cross section geometry on medium and maximum velocity ratio in open-channel flow, J. Hydraul. Eng. 142 (1) (2016), 06015015.
[24] R. Daneshfaraz, A. Ghaderi, A. Akhtari, S. Di Francesco, On the effect of block roughness in ogee spillways with flip buckets, Fluid 5 (4) (2020) 182.
[25] P. Parsamehr, A. Kuriqi, D. Farsadizadeh, A.H. Dalir, R. Daneshfaraz, R.M. Ferreira, Hydraulic jump over an adverse slope controlled by different roughness elements, Water Resour. Manag. 36 (14) (2022) 5729–5749.
[26] M. Paneru, C. Priest, J. Ralston, R. Sedev, Electrowetting of ionic liquids on teflon AF1600 in ambient hexadecane, J. Adhes. Sci. Technol. 26 (12–17) (2012) 2047–2067.
[27] P. Muthiah, S.H. Hsu, W. Sigmund, Coaxially electrospun PVDF− teflon AF and teflon AF− PVDF Core− sheath nanofiber mats with superhydrophobic properties, Langmuir 26 (15) (2010) 12483–12487.
[28] J.Y. Lu, J.H. Hong, C.Y. Wang, K.Z. Lee, H.C. Yang, Measurement and simulation of turbulent flow in a steep open-channel with smooth boundary, J. Chin. Inst. Eng. 26 (2) (2003) 201–210.
[29] T. Zhao, L. Jiang, Contact angle measurement of natural materials, Colloids Surf. B Biointerfaces 161 (2018) 324–330.
[30] A. Dotan, H. Dodiuk, C. Laforte, S. Kenig, The relationship between water wetting and ice adhesion, J. Adhes. Sci. Technol. 23 (15) (2009) 1907–1915.
[31] Y. Nakayama, Introduction to Fluid Mechanics, Butterworth-Heinemann, 2018.
[32] T. Heckenthaler, S. Sadhujan, Y. Morgenstern, P. Natarajan, M. Bashouti, Y. Kaufman, Self-cleaning mechanism: why nanotexture and hydrophobicity matter, Langmuir 35 (48) (2019) 15526–15534.
[33] M.I. Hossain, A. Ali, V. Bermudez Benito, B. Figgis, B. Aïssa, Anti-soiling coatings for enhancement of PV panel performance in desert environment: a critical review and market overview, Materials 15 (20) (2022) 7139.
[34] H. Schlichting, K. Gersten, Boundary-layer Theory, Springer, 2016.
[35] L. Prandtl, Meteorogische an wendung der stromungslehre, Beitr. Phys. Atomosph 19 (1932).
[36] H.A. Einstein, The Bed-Load Function for Sediment Transportation in Open Channel Flows (No. 1026), US Department of Agriculture, 1950.
[37] G.H. Keulegan, Laws of Turbulent Flow in Open Channels, vol. 21, National Bureau of Standards, Gaithersburg, MD, USA, 1938, pp. 707–741.
[38] P.M. Steffler, N. Rajaratnam, A.W. Peterson, LDA measurements in open channel, J. Hydraul. Eng. 111 (1) (1985) 119–130.
[39] I. Nezu, W. Rodi, Open-channel flow measurements with a laser Doppler anemometer, J. Hydraul. Eng. 112 (5) (1986) 335–355.
[40] M.S. Kirkgöz, Turbulent velocity profiles for smooth and rough open channel flow, J. Hydraul. Eng. 115 (11) (1989) 1543–1561.
[41] A.H. Cardoso, W.H. Graf, G. Gust, Uniform flow in a smooth open channel, J. Hydraul. Res. 27 (5) (1989) 603–616.
[42] Z. Dong, X. Liu, X. Wang, Aerodynamic roughness of gravel surfaces, Geomorphology 43 (1–2) (2002) 17–31.
[43] C.E. Shannon, A mathematical theory of communication, Bell Syst. Tech. J. 27 (3) (1948) 379–423.
[44] C.L. Chiu, Entropy and 2-D velocity distribution in open channels, J. Hydraul. Eng. 114 (7) (1988) 738–756.
[45] C.L. Chiu, Velocity distribution in open channel flow, J. Hydraul. Eng. 115 (5) (1989) 576–594.
[46] I. Nezu, H. Nakagawa, Turbulence in Open-Channel Flows, A. A. Balkema Publishers, Brookfield, Vt, 1993.